

## APS BEAM STABILITY STUDIES AT THE 100-NANORADIAN LEVEL\*

G. Decker, B.X. Yang, R. Lill, H. Bui, Advanced Photon Source  
Argonne National Laboratory, IL 60439, USA

### Abstract

Recent developments at the Advance Photon Source (APS) in the area of high-resolution beam position monitoring for both the electron and x-ray beams has provided an opportunity to study beam motion well below the measurement threshold of the standard suite of instrumentation used for orbit control. The APS diagnostics undulator beamline 35-ID has been configured to use a large variety of high-resolution beam position monitor (BPM) technologies. The source-point electron rf BPMs use commercially available Libera Brilliance electronics from Instrumentation Technologies, together with in-house-developed field-programmable gate-array-based data-acquisition digitizing broadband (10 MHz) amplitude-to-phase monopulse receivers. Photo-emission-based photon BPMs are deployed in the 35-ID front end at distances of 16 and 20 meters from the source, and a prototype x-ray fluorescence-based photon BPM is located at the end of the beamline, approximately 39 meters from the source. Detailed results describing AC noise studies will be provided.

### INTRODUCTION

Shown in Figure 1 is the experimental arrangement of diagnostics associated with the APS 35-ID undulator source point.

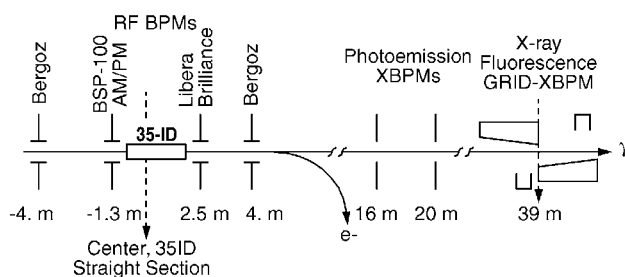


Figure 1: Array of beam position monitoring diagnostics used for beam stability studies at APS 35-ID.

This particular arrangement is unique in that 5 different BPM technologies located at 7 different locations along the beamline are all poised to provide quantitative measurements of beam position and pointing angle with unprecedented resolution. The work described in this paper is an extension of work started in 2009 in collaboration with researchers assessing BPM technologies for the NSLS-II facility now under construction [1].

### RF BEAM POSITION MONITORING

Near the source point, both narrowband and broadband rf BPM electronics are used to monitor the electron beam. Closest to the undulator, capacitive button pickup electrodes are mounted on the small-gap insertion-device vacuum chamber in sets of four, each with 4-mm diameter: two buttons above and two below the accelerator mid-plane at each station. The vacuum chamber vertical aperture is 8 mm; these pickup electrodes have very high geometric sensitivity. The upstream electrodes are connected to an in-house-designed data acquisition system: the bunch signal processor BSP-100, a field-programmable gate array (FPGA) module [2] samples a legacy broadband (10 MHz) amplitude-to-phase conversion BPM rf front end at a sample rate of 88 MS/sec, i.e., one fourth the ring's rf frequency. At the downstream station, commercial Libera Brilliance electronics from Instrumentation Technologies (Slovenia) are employed, which have recently been interfaced to the APS control system.

Due to the high sample and processing rates made possible by (FPGA) technology, and AC noise floor approaching  $1 \text{ nm}/\sqrt{\text{Hz}}$  are realizable. Shown in Figure 2 are data showing the performance of commercial Libera Brilliance BPM electronics in contrast to the BSP-100 data acquisition attached to the APS broadband rf BPM front end. By using a four-way splitter from a single button pickup, the noise floor was determined and compared with actual levels of (closed-loop) beam motion in the 35-ID straight section. Horizontal (X) and vertical (Y) data together with the noise floor are plotted as cumulative rms motion by integrating the power spectral density for turn-by-turn data using data sets of 0.5 and 1 second duration for the Libera and BSP-100 module, respectively. The straight lines indicate reference white noise levels.

In addition to the broadband BPMs, located  $\pm 4$  meters from the center of the insertion device straight section, are sets of four 1-cm-diameter pickup electrodes mounted on standard large-aperture (4 cm x 8 cm elliptical) vacuum chambers. Attached to these pickup electrodes are commercial narrowband Bergoz multiplexed BPM electronics which were installed c. 2000.

### PHOTOEMISSION-BASED PHOTON BPMS

In the beamline front end at 16.35 and 20 meters downstream of the undulator source point are photo-emission-based photon BPMs [3]. Due to small apertures in the front end, the detector located at 16.35 meters provides both horizontal and vertical position readbacks,

\*Work supported by U.S. Department of Energy, Office of Science, Office of Basic Energy Sciences, under Contract No. DE-AC02-06CH11357.

while the unit at 20 meters provides only vertical data. These type of detectors are known to be sensitive to stray sources of soft radiation emitted from nearby dipole, quadrupole and sextupole magnets. Sector 35 is unique in that the sector downstream of the source has not been realigned to reduce the stray radiation background [4].

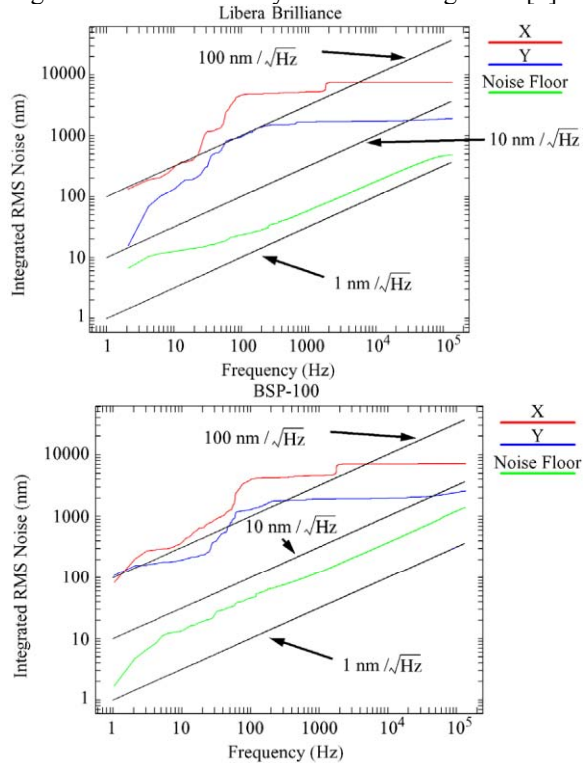


Figure 2: Integrated rms noise performance (green), with vertical (blue), and horizontal (red) beam motion for commercial Libera Brilliance BPM electronics (top) and the in-house BSP-100 module design (bottom), both attached to small-aperture pickup electrodes at the APS 35-ID source point.

### HARD X-RAY FLUORESCENCE-BASED PHOTON BPM

Finally, a prototype of a new type of x-ray BPM based on hard x-ray fluorescence from copper has been installed at the end of the 35-ID beam diagnostics beamline at a distance of 38.8 meters from the center of the undulator straight section [5]. This detector is sensitive only to very hard (> 8.98 keV) x-rays and as such is immune from systematic errors associated with stray soft radiation. Shown in Figures 3 and 4 are a photo and diagram indicating the operating principle of the grazing-incidence insertion device hard x-ray fluorescence BPM (GRID-XBPM).

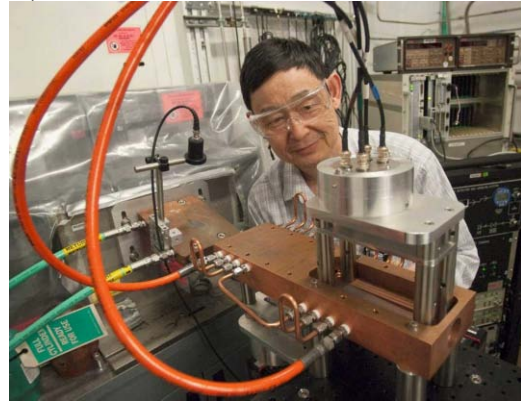


Figure 3: In-air prototype of grazing-incidence x-ray BPM.

In Figure 4, the x-ray beam, travelling left to right, first encounters a mask to protect downstream elements from misdirected beam. The XBPM proper is the center element, which resembles a mask, but sliced longitudinally with the two halves separated along the beam direction forming two ramps. X-rays striking the upstream ramp generate fluorescence x-rays that are detected with a pin-diode array below, while the

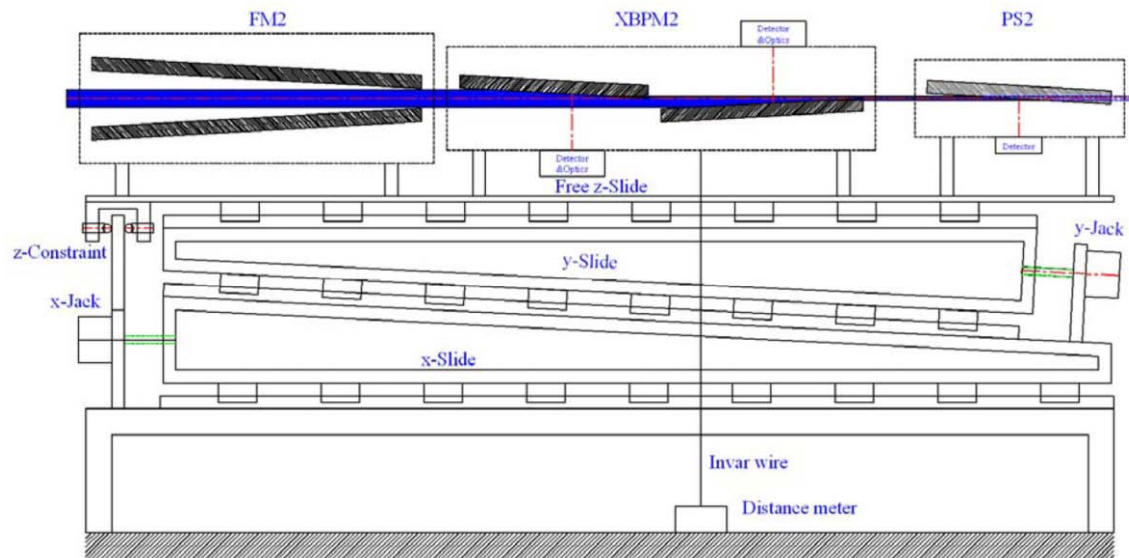


Figure 4: Diagram illustrating the operating principle of the grazing-incidence hard x-ray BPM.

downstream ramp produces x-rays that are detected with a similar array located above the midplane. In the simplest conception, the intensity difference between upstream and downstream ramps produces a signal proportional to the vertical displacement of the x-ray beam through the device. As instrumented (Figure 3), the x-ray footprint was imaged using a (large) pinhole in combination with a set of four pin diodes for each ramp.

At the downstream end of each ramp, a small rectangular trench of transverse dimensions 3 mm (horz.) by 1.5 mm (vert.) was cut along the beam direction to let the core of the x-ray beam pass. The monochromatic portion of the insertion device x-rays is located here. The far right-hand element of Figure 3 is a movable photon shutter which has been instrumented with a single pin diode to monitor the transmitted x-ray flux. This detector is actually above the midplane in the photo, where the beam travels right to left.

Shown in Figure 5 are gap scan data comparing signals from the 35-ID photoemission-type photon BPM (top) and the hard x-ray fluorescence-based detector. Because the former is sensitive to very soft photons, the background signals present at large gap are considerable and are highly variable from one blade to the next. In contrast, the fluorescence detector is essentially immune to soft radiation, demonstrating clean exponential response across a range in signal strength of a factor of 200.

### Hard X-ray BPM Calibration

Shown in Figure 6 are the photodiode currents resulting from scanning the detector across the beam (bottom) or scanning the beam across the detector using an asymmetric local closed-orbit angle bump centered on the 35-ID straight section (top). Horizontal response is on the left, and vertical on the right – note scales. For these data and that to follow, the detector was rotated by 90 degrees compared to Figure 3, for practical reasons (to allow higher heat load), effectively exchanging horizontal and vertical functionality. The abscissae for the beam scans were extrapolated from the two rf BPM channels closest to the source point, whose calibrations were carefully checked against a calibrated ring model.

With eight photodiodes to choose from, many permutations are possible to produce signals proportional to either vertical or horizontal beam position. In order to use the same electronics as for the traditional photoemission-type BPMs, two diodes from the upstream ramp were combined with two diodes from the downstream ramp to produce a single (x, y) pair of readbacks, referred to here as S36ID:P. This left a spare pair of diodes on the upstream ramp, one above and one below the midplane, and a second downstream pair. These resulted in two independent vertical readbacks, corresponding to channels S36ID:P2:Y and S36ID:P2:X (normally P2 assumes top-bottom-left-right geometry vs. a diagonal arrangement for P1).

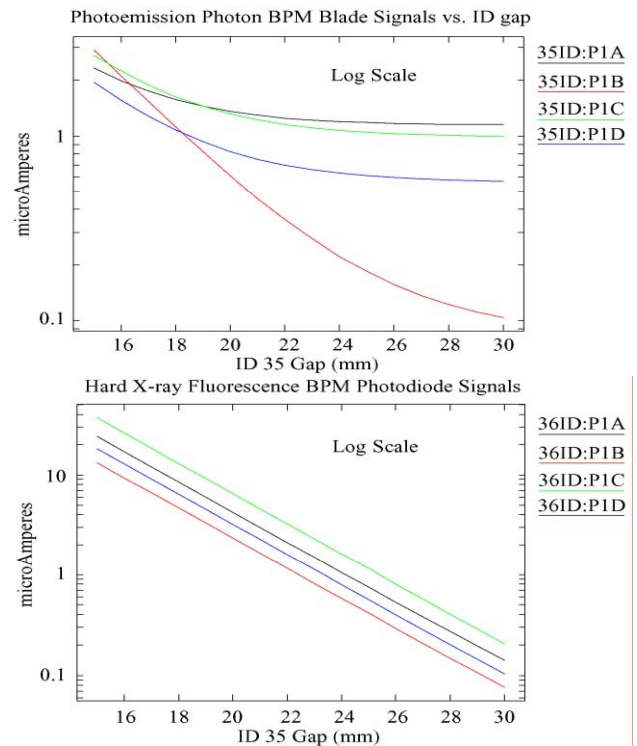


Figure 5: Comparison of gap dependence of photoemission style BPM (top) with x-ray fluorescence (bottom).

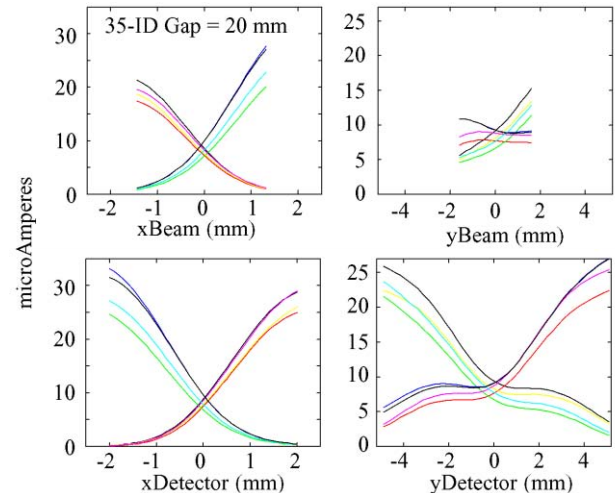


Figure 6: Beam scans (top) vs. detector scans (bottom).

Shown in Figure 7 are the resulting calibration curves, plotting difference over sum (e.g., top – bottom divided by their sum) as a function of transverse position. The beam scans were flipped left/right, and all data were shifted so as to be centered at (or at least near) the point of maximum slope. The interesting inflection point behavior for the vertical data is a consequence of the pass-through trench, which is oversized for this detector orientation.

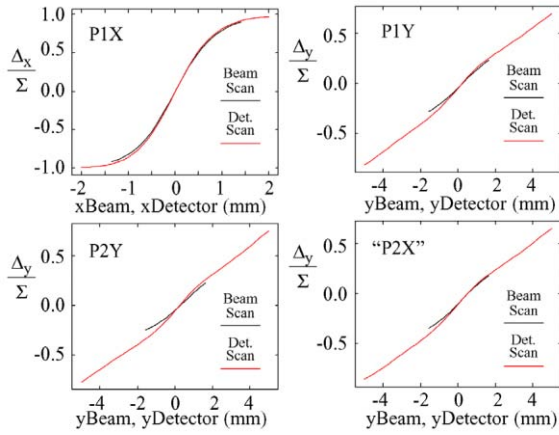


Figure 7: Calibration curves for photoemission-type hard x-ray BPM.

With the data of Figure 7 in hand, a numerical differentiation was performed, and the maximum slope provides the calibration factors desired (actually their inverse). Shown in Table 1 are the calibration factors (in mm) that are to be multiplied by the delta / sum ratio to produce position readbacks, in units of mm.

Table 1: Hard X-ray BPM Calibration Factors

Channel	Beam Cal.	Detector Cal.
S36ID:P1:X	0.8842 mm	0.8305 mm
S36ID:P1:Y	5.263 mm	4.538 mm
S36ID:P2:Y	4.987 mm	4.506 mm
“S36ID:P2:X”	5.490 mm	4.506 mm
S35ID:P1:X	3.682 mm	2.963 mm
S35ID:P1:Y	1.059 mm	0.1408 mm
S35ID:P2:Y	0.7843 mm	0.1348 mm

In this table, higher numbers imply lower sensitivity. The vertical calibration factors show a spread of + / - 5% for the calibration with beam, which is not seen for the detector calibration. This is likely due to shadowing effects of upstream apertures. Adjustments in the pinhole geometry together with reduction in the height of the pass-through slot are expected to improve vertical sensitivity in future designs. Data for the 35-ID photoemission BPM are included for completeness.

### CORRELATED DATA ACQUISITION

The APS real-time feedback system operates at a sample rate of 1.534 kHz and has access to a large number of readback and control points [6]. Among its many capabilities is an oscilloscope functionality allowing synchronous acquisition of up to 40 channels. Unfortunately, the Libera and BSP-100 boxes are not yet integrated with the real-time system. Because the ring model is so well known, it is straight forward to infer the readings at these locations’ pickup electrodes using a free betatron oscillation formula together with adjacent Bergoz

data, which are available to the real-time system. Shown in Figure 8 are comparisons of integrated spectra for Libera and Bergoz, with the Bergoz data interpolated from the betatron formula to the Libera location as just described.

As noted in the figure, this is an unfair comparison, for two reasons: first, the Bergoz electronics are mounted on a large-aperture vacuum chamber vs. Libera, which uses a small aperture and thus has higher geometric sensitivity. Further, at least in the vertical plane, the beta functions at both the real Bergoz location and the Libera location are quite small (< 5 m); the amount of real beam motion is very small to start with. The conclusion to be drawn from Figure 8 is that the Bergoz receivers do an adequate job of characterizing horizontal motion at the undulator source point, while vertically they are limited by noise, certainly with feedback running. The fact that the lowest left-hand Bergoz curve closely follows a straight line with slope 1/2 supports this hypothesis. Note that the Libera data start at 2 Hz because these plots were derived from a turn-by-turn data set with duration 0.5 seconds.

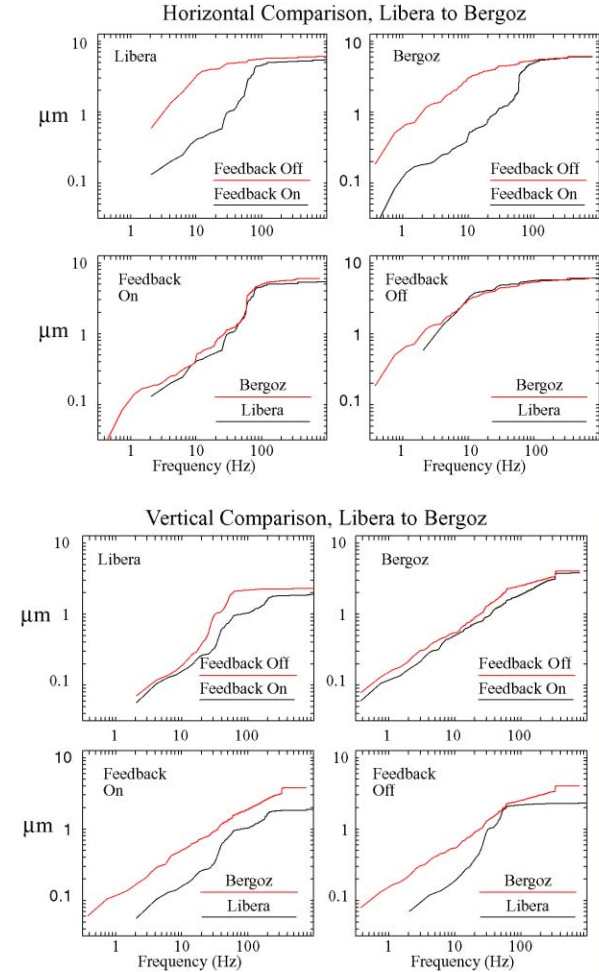


Figure 8: Unfair comparison of Libera vs. Bergoz data. Bergoz data interpolated to location of Libera pickups.

Shown in Figure 9 are integrated spectra for all BPMs along the 40-meter-long 35-ID beamline, vertically (above) and horizontally (below), with feedback on (right), and off (left). The rf BPMs at the source are in

red and black with the smallest integrated rms beam motion. Next noisiest are the front-end photoemission photon BPMs (UVBPM), and, at the end of the beamline, the hard x-ray fluorescence BPM (GRID XBPM) shows the largest amount of beam motion, as expected. With the exception of the Libera and BSP-100 vertical data, all data on each of the four panels were synchronous, from the same 1.5 kHz data set. Note the effect of the small vertical beta function at the source: there is 10 times as much beam motion at the end of the beamline compared to the source (with feedback off).

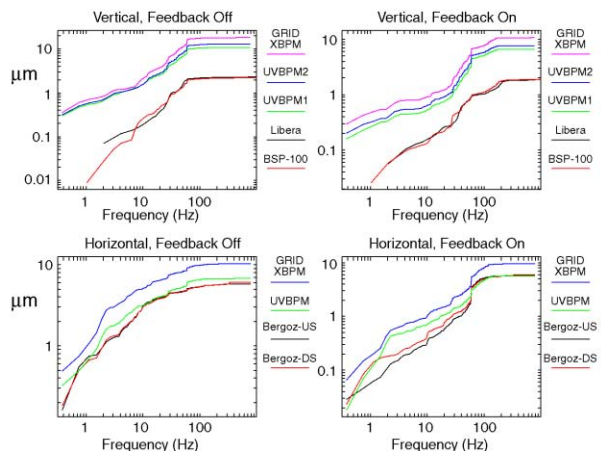


Figure 9: Integrated PSD data for BPMs along 35-ID.

As an example of the kinds of analyses that can be performed using the synchronous data provided by the real-time feedback system, shown in Figure 10 are vertical phase-space plots showing position at the various locations along the beamline on the horizontal axis, with vertical angle plotted on the vertical axis. The angle was calculated from photon BPMs UVBPM2 and the GRID-XBPM by taking their difference and dividing by their separation along the beamline (19 meters), on a sample-by-sample basis. In this particular case, angular motions cause the beam size to increase the further downstream one goes, and these small angular motions cannot be seen in this case using only (Bergoz) rf BPMs near the source.

One last example is that the two equivalent measures of vertical position at the end of the beamline, namely S36ID:P1:Y and S36ID:P2:X can be plotted against each other and fit to a straight line. The slope of this line was found to be 1.015 with feedback off and 1.028 with feedback on. More interesting is that the rms of the fit residual is a measure of instrumentation noise, equal to 2.36 or 2.48 microns, respectively. With a lever arm of 39 meters, this amounts to something like 60 nanoradians of angular resolution. Given the higher sensitivity in the horizontal plane, one can expect significantly better resolution there, with vertical improvements underway.

## SUMMARY

Studies at APS beamline 35-ID have validated a new type of photon BPM with very high AC and DC resolution. This detector was successfully included in

closed-loop feedback, and the beam could be steered very precisely by physically moving the mechanical translation stage upon which the detector was mounted. This mode of operation is being contemplated as part of the APS upgrade. A full in-vacuum design for a high-power version for insertion device beamline front ends is in progress.

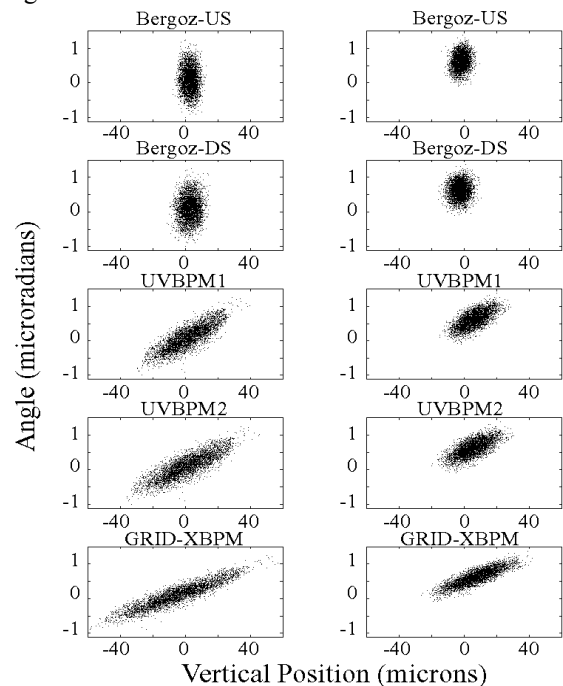


Figure 10: Vertical angle vs. position with feedback off (left) and on (right).

## REFERENCES

- [1] O. Singh, I. Pinayev, G. Decker, and B.X. Yang, "Comparative Studies of RF Beam Position Monitor Technologies for NSLS-II," DIPAC'09, Basel, Switzerland, July 2004, MOPD16, p. 80 (2009); <http://www.JACoW.org>.
- [2] H. Bui, G. Decker, R. Lill, A. Pietryla, W.E. Norum, "Performance of FPGA-Based Data Acquisition for the APS Broadband Beam Position Monitor System," BIW'08, Tahoe City, CA, USA, TUPTPF001, p. 80 (2009); <http://www.JACoW.org>.
- [3] G. Decker and O. Singh, "Orbit Feedback Using X-ray Beam Position Monitoring at the Advanced Photon Source," ICALEPCS'01, San Jose, CA, USA, WECI001, p. 249, <http://www.JACoW.org>.
- [4] G. Decker, O. Singh, "Method for Reducing X-ray Background Signals from Insertion Device X-ray Beam Position Monitors," PRST-AB 2(11), 112801 (1999).
- [5] B.X. Yang et al., "High-Power Hard X-ray Beam Position Monitor Development at the APS," these proceedings.
- [6] J. A. Carwardine and F.R. Lenkszus, "Real-Time Orbit Feedback and the APS," BIW'98, AIP Conference Proceedings No. 451, p. 125 (1998).